IOP PUBLISHING JOURNAL OF PHYSICS D: APPLIED PHYSICS

J. Phys. D: Appl. Phys. **42** (2009) 015203 (8pp) doi:10.1088/0022-3727/42/1/015203

Metastable oxygen atom velocity and temperature in supersonic CO_2 plasma expansions

S Mazouffre[1] **and E Pawelec**[2]

[1] ICARE, CNRS, 1c Av. de la Recherche Scientifique, 45071 Orléans, France
[2] Department of Physics, University of Opole, Oleska 48, Opole, Poland

E-mail: stephane.mazouffre@cnrs-orlean.fr

Received 19 June 2008, in final form 20 June 2008
Published 10 December 2008
Online at stacks.iop.org/JPhysD/42/015203

Abstract
Radial and axial velocity distribution functions of $^5S_2^o$ metastable oxygen atoms were obtained by way of resonant laser induced fluorescence spectroscopy at 777.19 nm in rarefied supersonic plasma jets produced from pure CO_2 and CO_2–N_2 gas mixtures. The N_2 seeded fraction is 3% in volume in order to mimic the Martian atmosphere composition. The measured lineshapes allow computation of the mean radial velocity and the perpendicular temperature, with respect to the jet axis, as well as the mean axial velocity and the parallel temperature. With an arcjet plasma source input power of 6.5 kW, the metastable O(^{5}S) atom axial velocity is around 4500 m s^{-1} and the atom perpendicular temperature reaches 4500 K at the nozzle outlet. Under identical voltage and current conditions, a small addition of N_2 does not change the measured values, i.e. it does not modify the overall energy balance. Distribution of flow parameters along both the radial and the axial directions reveals the existence of a barrel shock wave and a stationary shock front, which originate in shock wave regular reflexion. Flow properties, shock wave structure, departure from thermal equilibrium and impact of the applied power are debated for the two gas mixtures. Finally, the capacity of supersonic plasma expansions to simulate interplanetary probe entry into the Martian atmosphere is discussed in the light of experimental outcomes.

1. Introduction

An ambitious exploration program of Mars is being considered by space agencies for the next decades [1, 2]. A common objective of all projects is to go beyond robotic missions by preparing sample return missions and ultimately manned missions to the red planet. Therefore, numerous efforts are devoted nowadays all around the world to design and build low-cost, reliable and safe space vehicles. Low-pressure supersonic plasma jets containing CO_2 molecules are used to simulate entry of space probes in the upper layers of the Martian atmosphere [3], as the latter consists of 95.3% carbon dioxide, 2.7% nitrogen, 1.6% argon, and contains traces of oxygen and water vapour. From a technological standpoint, high enthalpy CO_2 jets are used to verify the proper design of thermal shields. From a more fundamental viewpoint, investigation of CO_2 plasma expansions allows collection of a vast dataset necessary to better understand the formation of chemically reactive species—radicals, ions and rovibrationally excited molecules—as well as non-equilibrium effects behind the bow shock wave formed around a space vehicle during the high-speed high-altitude entry stage [4]. Indeed, the properties of the complex plasma medium that surrounds a spacecraft have a drastic impact upon the flight conditions. In the worst case, energy transfer between the plasma and the vehicle can lead to destruction of the latter. To avoid failure of the mission, numerical simulations of spacecraft trajectory into the Martian atmosphere must be carried out with an accurate modelling of the plasma characteristics in terms of particle densities, temperatures, ionization degree and radiative flux [5, 6]. Hence the necessity to validate models of plasma formation and flow. One way to achieve this objective is to compare computational outcomes to experimental data obtained with rarefied supersonic flows. Several experiments have been carried out over the past few years in plasma wind tunnel with CO_2. The large amount of acquired data mostly corresponds to density, temperature and heat flux. Electron properties are measured by means of Langmuir probes [7].

Flow composition is given by mass spectrometry. Emission spectroscopy is used to gather information about neutrals and ions temperature and to assess radiative flux in various spectral ranges. Heat flux is usually determined from enthalpy probe measurements. Most of the time, the flow velocity is estimated from thermodynamics and fluid dynamics calculations. Only a few attempts to measure the velocity were performed in low-pressure plasma jets by means of a Pitot tube and Mach probes [7], in spite of flow disturbances. However, the gas velocity is a relevant quantity as it defines the flight domain that is covered by the experimental facility. Moreover, the kinetic energy is the main energy source for chemistry and radiation production throughout the bow shock wave and the boundary layer that surrounds a space probe.

In this contribution, we show that near infrared diode laser induced fluorescence (LIF) spectroscopy is perfectly suited to monitor the velocity distribution function (VDF) of metastable oxygen atoms in weakly-ionized CO_2 plasma expansions. The possibility to detect oxygen atoms at 777 nm in a plasma by way of low-power continuous-wave LIF spectroscopy was demonstrated by Baer and co-workers in 1993 [8]. Ten years later, laser absorption spectroscopy at 777 nm was used to measure the density of atomic oxygen in an argon–oxygen arcjet plume [9]. First, the LIF technique allows one to achieve a high spatial resolution, which is necessary to resolve steep gradients that exist across shock waves. Second, near IR radiation can easily be generated with compact diode laser that are easy to handle and to operate. Moreover, cw coherent light sources offer a high spectral resolution, the source bandwidth being much smaller than the transition linewidth. Here, velocity and temperature of $^5S_2^o$ metastable oxygen atoms in the axial and the radial directions are inferred from the Doppler shift and the Doppler broadening of the fluorescence spectral profile, respectively. To the best of our knowledge, such quantities have never been measured in CO_2 free plasma jets with a non-intrusive diagnostic technique. Long-lived $^5S_2^o$ oxygen atoms are created inside the nozzle in a high pressure region where the numerous momentum transfer and metastability exchange collisions warrant a strong mixing between metastable and ground-state oxygen atoms. Therefore the $^5S_2^o$ oxygen atom VDF images the ground-state atom one. From the measurements, the distribution of the flow parameters is obtained in parallel and perpendicular directions with respect to the jet centreline for CO_2 and CO_2–N_2 gas mixture. The shock wave structure, departure from thermal equilibrium and the influence of the discharge current will be debated. Furthermore, the capability of supersonic plasma expansions to simulate probe entry into the Martian atmosphere will be questioned.

2. Experimental arrangement

2.1. Plasma sources

The plasma source used in the ground-test facility, the so-called SR5 wind tunnel, is a water-cooled vortex stabilized dc-arc torch [4]. The torch is equipped with a zirconium cathode when oxidizing gases are burned and with a convergent–divergent copper nozzle that acts as a grounded anode. The cathode to anode gap is 1 mm. The length of the divergent part is 5.1 cm and the exit diameter of the nozzle is 4.9 cm. The arc extends from the tip of the cathode through a 4 mm diameter molybdenum throat and attaches diffusely to the nozzle. The plasma torch can be operated in a wide range of currents and flows, and it can be run for several hours, the lifetime being determined by the cathode wear. Gases are fed through mass flow controllers directly into the cathode area. The torch is mounted on an arm that can be moved in the vertical and the horizontal directions.

Table 1. Normal operating conditions.

Gas	Φ_{CO_2} (slm)	Φ_{N_2} (slm)	I (A)	U (V)	p_{back} (Pa)	η	h (kJ g^{-1})
CO_2	13.32	0	100	65	4	0.66	9.4
CO_2–N_2	14.36	0.45	70	67	4	0.61	6.0

A thermal plasma is created in CO_2 gas, pure or seeded with a small amount of molecular nitrogen to reproduce the Martian atmosphere composition. Subsequently the plasma expands from the torch nozzle into a low-pressure steel vessel. The vacuum chamber is 4.3 m long and has a diameter of 1.1 m. The pumping system is made of three large Roots blower pumps evacuated by a set of roughing pumps to ensure a residual pressure around 1 Pa during operation. Standard operating conditions for this experiment are summarized in table 1. The efficiency as well as the specific enthalpy are assessed from measurement of the power given to the gas.

A detailed description of the physics of rarefied supersonic plasma jets is available elsewhere [10, 11]. As the plasma expands through a convergent–divergent nozzle from a high pressure region into a low-pressure region, a well-defined free jet shock wave structure is produced. The plasma first flows supersonically: the Mach number reaches 1 at the nozzle throat and the flow is supersonic in the divergent portion. In this flow domain, the temperature drops and the drift velocity increases due to energy conservation. In the meantime, the particle density along a streamline decreases because of the increase in the jet diameter. In the case of an underexpanded jet, the flow domain is limited by a barrel shock wave behind the nozzle exit. At some distance from the source, depending among others upon the background pressure, the side shock waves interact with one another on the jet axis. Depending upon the exit Mach number and the rarefaction degree, two shock wave configurations are then possible as explained by Graur and co-workers [12]. A Mach disc associated with an oblique reflected shock can be created through which the flow undergoes a supersonic to subsonic transition: Mach reflection. Under specific conditions, i.e. a large Mach number and a high level of rarefaction, the Mach disc vanishes and the flow experiences a supersonic to supersonic transition with a slight decrease in the Mach number magnitude: regular reflection. The latter process can occur several times over appreciable distances leading to the appearance of several stationary expansion cells. The transition between regular and Mach reflection of shock waves in a steady gas flow has been extensively studied [13, 14].

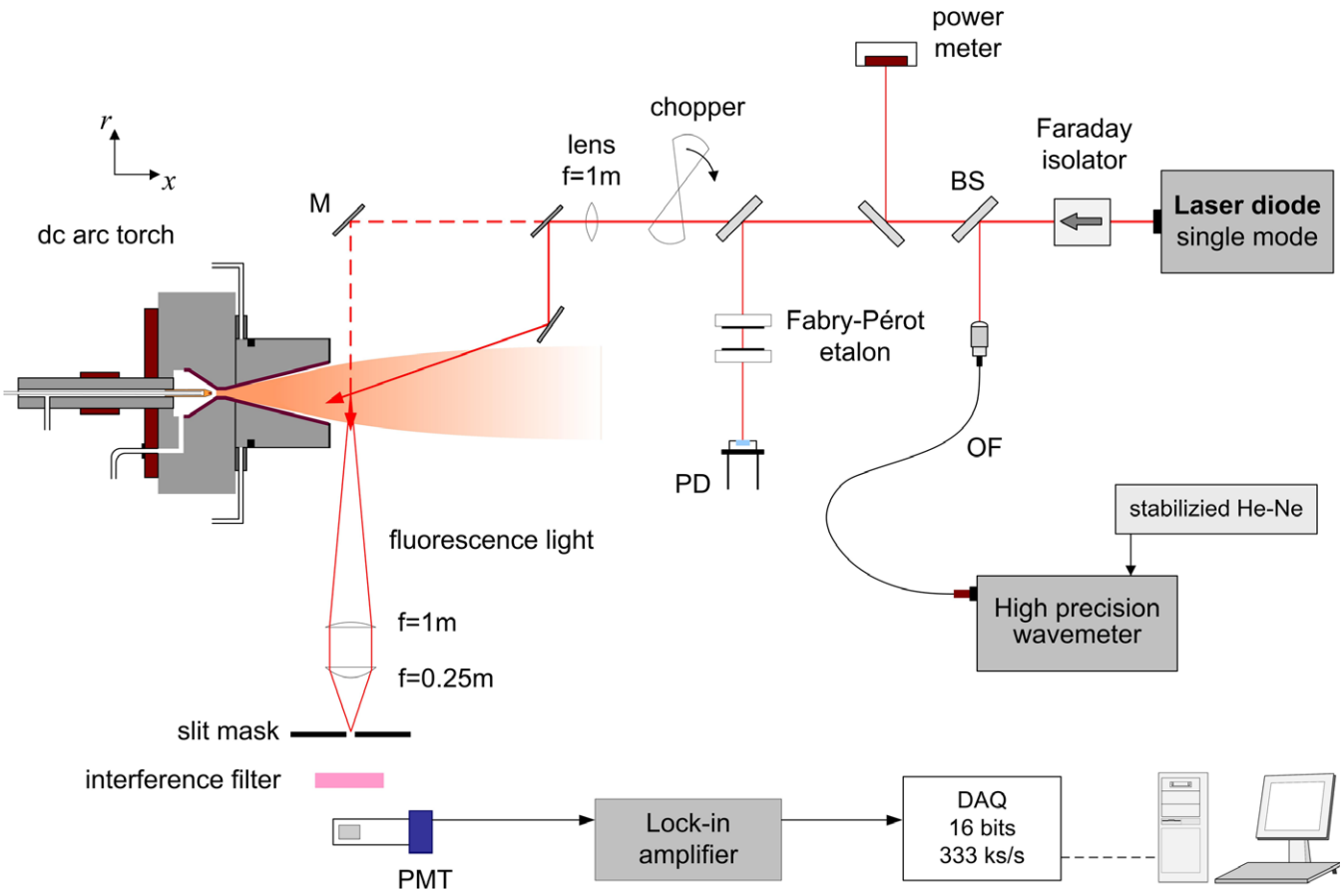

Figure 1. Schematic view of the cw-LIF setup used to detect metastable oxygen atoms. The laser beam can be directed either perpendicular or sideways (30°) with respect to the plasma jet centreline.

(This figure is in colour only in the electronic version)

Beyond the overall shock region, the plasma flows subsonically at constant static pressure.

2.2. *Optical bench*

A schematic of the optical bench is depicted in figure 1. A single mode tunable external cavity diode laser (Sacher TEC 500) delivers several milliwatts of horizontally polarized near-infrared radiation around 777 nm with a bandwidth of 10 MHz. A Faraday isolator prevents any reflected beam of light from entering back into the laser cavity. A small fraction of the beam is sent to a high precision calibrated wavemeter to monitor the laser light frequency with an absolute accuracy of 100 MHz. Another beam splitter directs a small part of the laser into a 0.99 GHz Fabry–Pérot etalon to monitor mode structure and to ensure that no mode hop occurs during operation. The mode-hop free tuning range of the laser is typically 10 GHz with voltage–current coupling. The laser beam power is also continuously monitored. Two excitation configurations are possible as shown in figure 1. In one configuration using a plane broadband dielectric mirror located inside the vacuum chamber, the laser beam propagates opposite to the plasma flow direction at a $\theta = 30^\circ$ angle with respect to the jet axis. In another configuration the beam is directed perpendicularly to the flow direction. In both cases a 1 m focal distance lens is used to focus the beam. The beam diameter is estimated to be around 2 mm in the probed zone. The laser light is chopped at a frequency of about 350 Hz and the LIF signal is detected on a horizontal axis normal to both excitation directions. The signal is collected with two lenses and imaged onto a $0.5 \times 1\,\mathrm{mm}^2$ slitmask. The slitmask determines the spatial resolution. The magnification is equal to 4; hence the object dimensions are $2 \times 4\,\mathrm{mm}^2$, small enough to resolve any gradient scale length [15]. A 10 nm bandwidth interference filter centred at 780 nm allows one to isolate the fluorescence radiation emitted at 777.2 nm from the remainder of the spectrum. Phase-sensitive detection is used to discriminate the fluorescence light from the intrinsic plasma emission. The signal delivered by the light detector is analysed with a lock-in amplifier which is synchronized to the chopper frequency. All signals are recorded simultaneously with a 16 bits 333 kHz analog-to-digital converter.

All measurements presented in this contribution correspond to excitation of the oxygen atom $^5S_2^o$ metastable level as the laser frequency is scanned over the $3s \rightarrow 3p$ transition at $\lambda = 777.1944$ nm. A recorded spectral profile is a direct measurement of the local metastable oxygen atom FDV. Stark and pressure broadening can be neglected in view of, respectively, the low electron density [16][3] and the low gas pressure [17].

[3] The electron density was measured on-axis at the nozzle outlet with Langmuir probes; one finds $n_e = 2 \times 10^{19}\,\mathrm{m}^{-3}$ for CO_2.

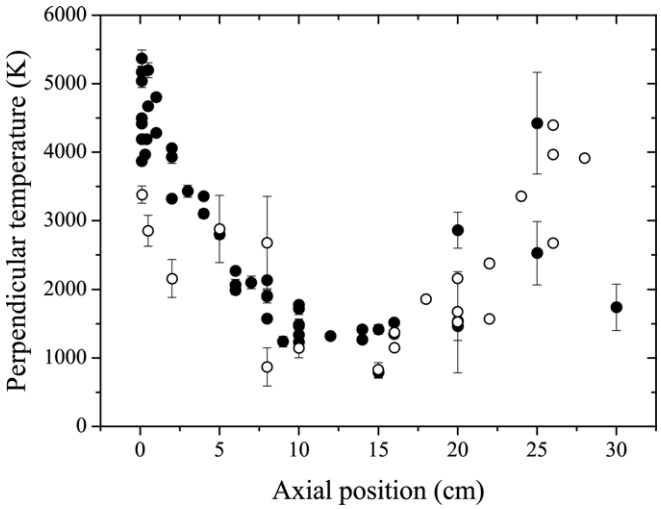

Figure 2. On-axis profile of the oxygen atom perpendicular temperature $T_\perp$ for a CO_2 (full circle) and a CO_2–N_2 (open circle) plasma expansion. The position $x = 0$ corresponds to the nozzle exit plane.

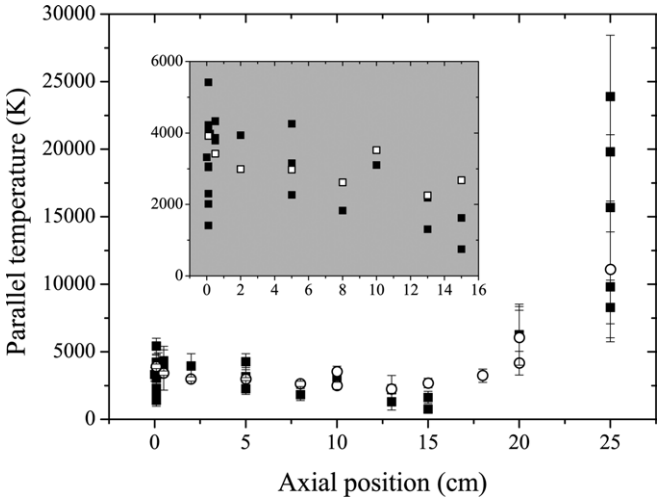

Figure 3. On-axis profile of the oxygen atom parallel temperature $T_\parallel$ for a CO_2 (full square) and a CO_2–N_2 (open square) plasma expansion. The inset panel displays the section of the data ahead of the normal shock wave.

Moreover, the laser power deposited inside the measurement volume was kept below 3 mW to limit power broadening [18]. Throughout the plasma jet supersonic domain, metastable O(^{5}S) atom VDFs exhibit a Gaussian shape that is a sign for local thermodynamic equilibrium. Across side and front shock waves, departure from equilibrium is expected [19, 20], however, the poor signal-to-noise ratio is unable to distinguish any change in the VDF shape. In order to infer the quantities of interest, a Gaussian curve was fitted to each VDF. The O(^{5}S) atom mean velocity, respectively the temperature, in the laser beam wave vector direction is then given by the Doppler shift, respectively the Doppler width [21]. Associated error bars shown in every graph were computed from the standard error on the Gaussian fit parameter value.

3. Oxygen atom flow properties along the jet axis

3.1. Temperature profiles

The development along the jet centreline of the perpendicular temperature $T_\perp$, associated with the distribution function of the metastable atom radial velocity component—with respect to the jet axis—is plotted in figure 2 for the two gas mixtures. Note that $x = 0$ corresponds to the nozzle exit. The temperature first decreases due to the supersonic expansion of the plasma jet. The observed abrupt rise of $T_\perp$ indicates the presence of a diffuse stationary shock wave at $x = 15$ cm through which kinetic energy is converted into thermal energy. Formation of the shock wave is discussed in section 3.2. The axial profile of the parallel temperature $T_\parallel$, associated with the distribution function of the O(^{5}S) atom axial velocity component, is shown in figure 3. The shape of the $T_\parallel$ profile resembles the one of $T_\perp$ as they are both directly connected with the jet shock wave structure.

Due to the rarefaction effect, at a certain location inside the divergent section of the nozzle the number of collisions becomes too low to maintain equilibrium between the two temperatures that diverge from each other as the expansion process proceeds with $T_\perp < T_\parallel$ as explained in [10] and as observed, e.g. in argon plasma expansions [15, 19, 20]. At the nozzle outlet and across the supersonic flow domain, departure from thermal equilibrium is solely observed for a CO_2–N_2 mixture. At the nozzle exhaust one finds out $T_\perp = 3200$ K and $T_\parallel = 4000$ K. In the case of a pure CO_2 plasma expansion, $T_\perp$ and $T_\parallel$ are identical for all positions ahead of the normal shock wave, taking into account error bars and measurement spread. The apparent thermal equilibrium observed with CO_2 is likely to be due to the instability of the arcject that is revealed by the large data spread, as can be seen in figure 2.

The stationary shock wave region starts at $x = 15$ cm for the two gas compositions as indicated by the sudden jump in temperature, see figures 2 and 3. In the shock region, the magnitude of $T_\parallel$ reaches ~17000 K and ~11000 K for a CO_2 an a CO_2–N_2 jet, respectively, as shown in figure 3. Note that error bars are large. The rise in the perpendicular temperature value is less pronounced, nonetheless $T_\perp$ reaches about 4000 K. The high temperature is a direct consequence of energy conversion during collision events. For an oxygen atom, assuming full energy conversion, a temperature of 17 000 K, respectively, 11 000 K, corresponds to a velocity of 4200 m s^{-1}, respectively, 3400 m s^{-1}. These two numbers are compatible with values of the O(^{5}S) atoms velocity measured ahead of the shock wave, see figure 4. This simple calculation indicates that the plasma flow strongly slows down when the jet particles collide with the background gas particles.

The complete on-axis shock wave structure could not be revealed as the fluorescence signal vanishes when the x position is above ~25 cm. The decrease in signal intensity has two main origins. First, the finite radiative lifetime $\tau_r = 91 \pm 5\,\mu$s of O(^{5}S) atoms allows them to cover a mean length of 36 cm at 4000 m s^{-1} in a collisionless medium before dissapearing [22]. As no energy is supplied to the plasma behind the nozzle exhaust, the metastable oxygen atom density slowly decays. Note that three-particle recombination

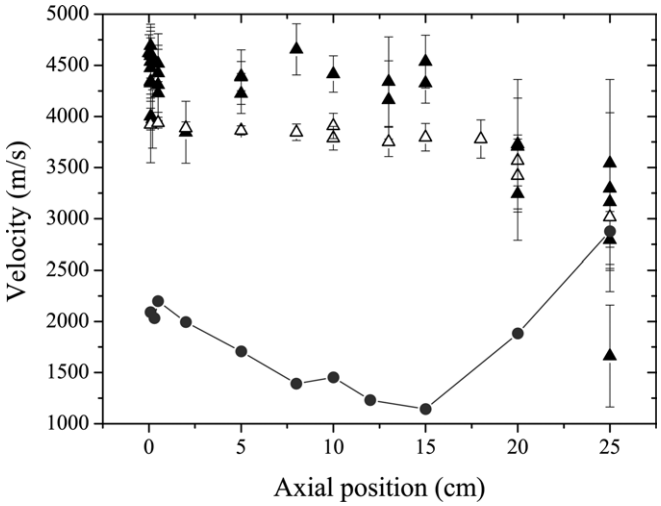

Figure 4. Development along the plasma jet centreline of the metastable oxygen atom axial velocity component v_x for pure CO_2 gas (full triangle) and a CO_2–N_2 mixture (open triangle). Also shown is the thermal speed calculated from the mean kinetic temperature T for a CO_2 jet.

of O^+ ions can produce $O(^5S)$ atoms; however, it is a weak process at low pressure. Second, $O(^5S)$ atoms disappear when colliding with atoms and molecules like O_2, CO and CO_2 of which the density increases in the shock wave region [23]. Deexcitation due to electron impact may also play a role in the shock wave.

3.2. Velocity distribution and shock wave

The evolution of the axial velocity component v_x along the jet centreline is shown in figure 4 for the two gas mixtures. The axial velocity v_x is computed from the measured velocity v_m by taking into account the sight angle θ

$$v_x = \frac{v_m}{\cos(\theta)}. \tag{1}$$

Also shown in figure 4 is the local oxygen atom thermal speed v_{th} calculated from the mean kinetic temperature T. For a rarefied flow with cylindrical symmetry T is given by

$$T = \tfrac{1}{3}(2T_\perp + T_\parallel). \tag{2}$$

The mean thermal speed reads

$$v_{th} = \sqrt{\frac{8k_B T}{\pi m}}, \tag{3}$$

where k_B is the Boltzmann constant and m is the mass of the species. Contrary to the speed of sound, the thermal speed does not depend on the specific heat ratio γ, which is always difficult to estimate in the case of a plasma generated from a molecular gas. The two approaches anyway give similar results. Throughout this paper the Mach number M is associated with the molecular speed ratio s:

$$M \approx s = \frac{v_x}{v_{th}}. \tag{4}$$

The on-axis profiles of the axial velocity component displayed in figure 4 for a CO_2 and a CO_2–N_2 plasma naturally reveal the existence of a stationary shock wave across which the flow experiences a deceleration through a pressure gradient that originates in a compression effect. Only one standing shock wave is visible in figure 4 at $x \approx 15$ cm as metastable $O(^5S)$ atoms cannot be detected behind $x \approx 30$ cm. Here, the shock wave finds its origin in the regular reflexion phenomenon: no Mach disk is formed and the flow undergoes a supersonic to supersonic transition across the shock wave with a speed ratio, or a Mach number, reduction [12–14]. The regular reflexion phenomenon is favoured under our experimental conditions according to numerical calculations carried out by Graur and co-workers to investigate transition conditions between Mach and regular reflexion of shock wave in underexpanded jets [12]. The regular reflexion occurs when, in the nozzle exit section, both the Mach number and the mean free path for momentum transfer λ are large. Under our conditions, at the nozzle exit the speed ratio reaches a value of about 2 for the two gas mixtures. The local mean free path for momentum transfer can in first order approximation be expressed as

$$\lambda = \frac{1}{n\sigma} \times \frac{v_x}{v_{th}}, \tag{5}$$

where n is the particle density and σ the corresponding cross-section. The CO_2 molecules must be considered here as they are the main species in the plasma jet. According to computer simulations carried out with a one-temperature fluid model, the CO_2 molecule density n_{CO_2} is around 10^{21} m^{-3} on-axis at the nozzle outlet with our operating conditions [17]. With a cross-section $\sigma = 37$ Å^2 for CO_2 at 2000 K [24], one finds $\lambda \approx 1$ cm. The magnitude of the dimensionless Knudsen number Kn can then be assessed at the torch outlet using the nozzle radius R as the characteristic length scale of the system

$$Kn = \frac{\lambda}{R}. \tag{6}$$

With $R = 2.45$ cm, Kn is 0.4, which means the flow approaches the rarefied regime. The values of M and Kn are therefore appropriate for the shock wave structure to be driven by the regular reflexion mechanism. Note that the step by step decay of the Mach number M that is due to the regular reflexion phenomenon was clearly observed in the same ground-test facility with an argon plasma expansion [15].

As can be seen in figure 4, the $O(^5S)$ atom axial velocity v_x stays constant along the jet axis in the supersonic flow domain for the two gas mixtures. As the thermal speed decreases from the nozzle exit all the way to the shock wave, the Mach number increases accordingly. It varies from 2.1 to 3.9 ahead of the shock wave for a pure CO_2 expansion and from 2.0 to 3.1 for a CO_2–N_2 mixture. In the two cases, the sum of the thermal energy and the kinetic energy on the flow centreline E_x is relatively high ahead of the shock. The quantity E_x reads

$$E_x = 3k_B T + \tfrac{1}{2} m v_x^2. \tag{7}$$

For oxygen atoms, the energy reaches 2.0 eV and 1.6 eV at $x = 15$ cm for a CO_2 and a CO_2–N_2 gas, respectively.

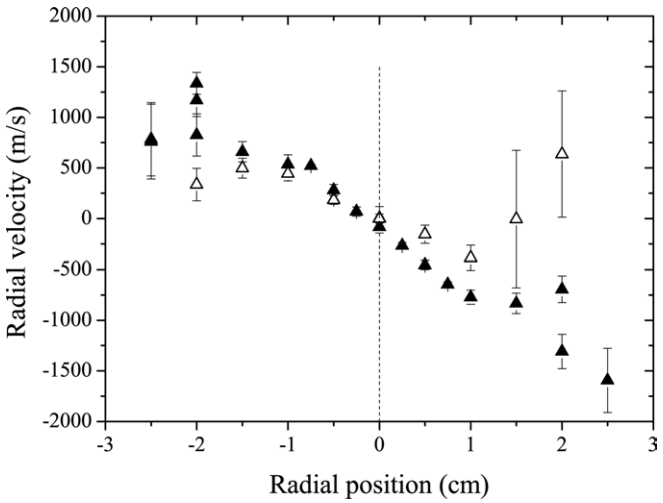

Figure 5. Radial profile at the nozzle exit of the metastable oxygen atom radial velocity component v_r for pure CO_2 gas (full triangle) and a CO_2–N_2 mixture (open triangle). The position $r = 0$ corresponds to the jet centreline.

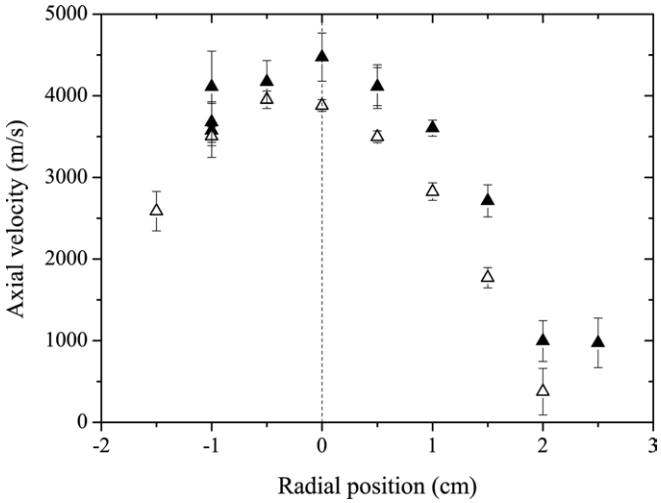

Figure 6. Radial profile at the nozzle exit of the metastable oxygen atom axial velocity component v_x for pure CO_2 gas (full triangle) and a CO_2–N_2 mixture (open triangle). The position $r = 0$ corresponds to the jet centreline.

The gap mostly originates in the difference in applied power, see table 1. Assuming that T and v_x are identical for CO_2 molecules, E_x would then reach 4.8 eV and 3.7 eV at 100 A and 70 A, respectively. Those numbers indicate that a lot of energy is available ahead of the shock wave region, all the more so energy is also stored in the form of molecular vibration and rotation as well as electronic excitation. A large fraction of the energy carried by the supersonic plasma flow is released inside the shock. A shock wave is naturally a region of strong pressure and velocity gradients; yet, it must in addition be considered as a chemically active area through which energy is exchanged, new species are formed and radiations are produced.

4. Jet structure at the nozzle outlet

Figures 5 and 6 show, respectively, the radial profile of the oxygen atom radial velocity v_r and the radial profile of the axial velocity v_x measured at the nozzle exit ($x = 1$ mm). As the laser light is shined with a sight angle $\theta = 30^\circ$ in parallel configuration, see figure 1, the axial velocity at position r is given by

$$v_x(r) = \frac{v_m(r) - v_r(r)\ \sin(\theta)}{\cos(\theta)}, \qquad (8)$$

where v_m is the measured velocity. At $r = 0$, i.e. on the jet axis, v_r is zero, hence one recovers equation (1). The radial velocity increases up to the barrel shock wave that corresponds to the supersonic flow domain boundary on side. As can be seen in figure 5, the lateral shock wave is located at $r = \pm 2$ cm for a CO_2 expansion and at $r \approx \pm 1.5$ cm for a CO_2–N_2 gas mixture. The radial profile of the $O(^5S)$ atom axial velocity components exhibits in the two cases a bell curve shape with a maximum velocity magnitude on the jet axis [10, 11], as shown in figure 6. The plasma flow is supersonic in the jet core and it becomes sonic, i.e. $v = \sqrt{v_x^2 + v_r^2} = v_{th}$, at $r \approx 2.5$ cm and at $r \approx 2$ cm ($v_{th} \approx 1600\ m\ s^{-1}$) for the 100 A case and the 70 A case, respectively. The radial position at which the plasma expansion becomes subsonic is close to the nozzle radius R, as the flow velocity must approach zero at the nozzle wall.

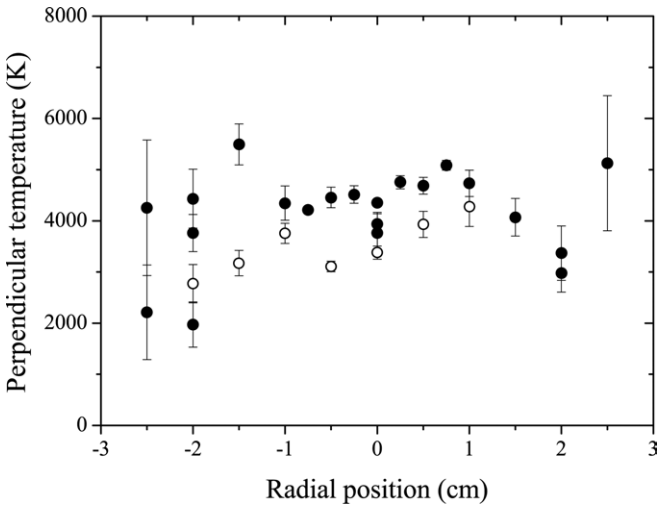

Figure 7. Oxygen atom perpendicular temperature $T_\parallel$ for a CO_2 (full circle) and a CO_2–N_2 (open circle) plasma as a function of the radial coordinate r at the nozzle exhaust.

Figures 7 and 8 show, respectively, the oxygen atom perpendicular and parallel temperature as a function of the radial position r at the nozzle exhaust for the two gas compositions. There is no clear structure in the parallel temperature profile, see figure 8. The perpendicular temperature does not depend on the radial coordinate inside the core of the plasma jet. It decreases across the barrel shock wave towards the background gas temperature.

5. Impact of the applied power

The enthalpy and the arc torch efficiency are displayed in figure 9 for the two gas mixtures. The two quantities are determined from the measurements of the temperature of

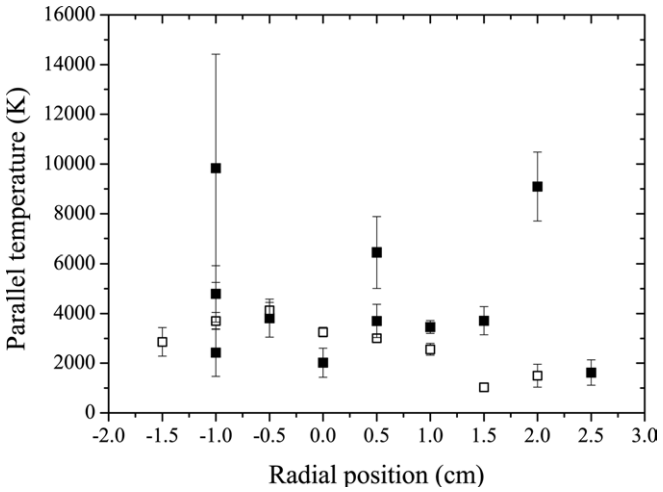

Figure 8. Oxygen atom parallel temperature $T_\perp$ for a CO_2 (full circle) and a CO_2–N_2 (open circle) plasma as a function of the radial coordinate r at the nozzle exhaust.

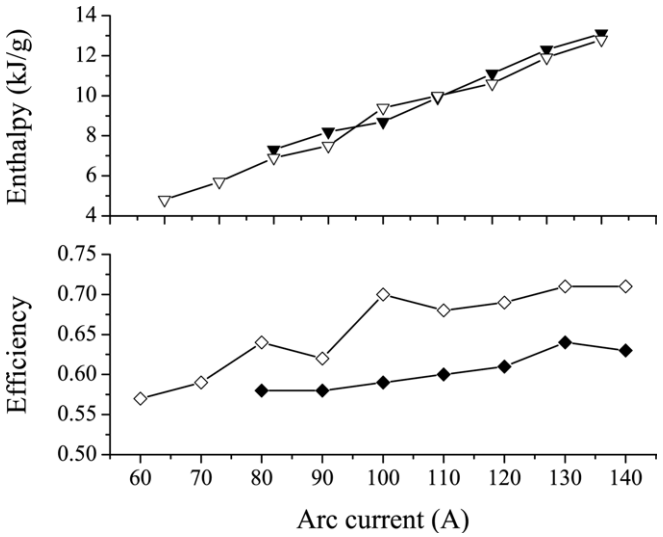

Figure 9. Enthalpy and efficiency as a function of the arc current for a CO_2 (full symbols) and a CO_2–N_2 (open symbols) plasma expansion. The arc voltage stays constant at (65 ± 2) V.

the cathode and anode cooling water. The voltage U stays unchanged at (65 ± 2) V whatever the current and the gas composition. At constant gas flow rate, the enthalpy increases with the input power, as expected. The observed higher efficiency for the CO_2–N_2 mixture is mostly due to the larger gas flow rate, see table 1.

The influence of the arc current upon the metastable oxygen atom parallel temperature and axial velocity component is shown in figure 10 for the two gas mixtures. The measurements were carried out at the nozzle exit ($x = 1$ mm) on the jet axis. The two quantities grow linearly with the applied power in the probed range in agreement with recent fluid simulations of the gas behaviour inside the nozzle [25]. As can be seen in figure 10, the addition of 3% N_2 has almost no influence on the values of $T_\parallel$ and v_x. Using the parallel temperature to compute v_{th}, the Mach number stays roughly unchanged with $M \approx 2$. A velocity in excess of

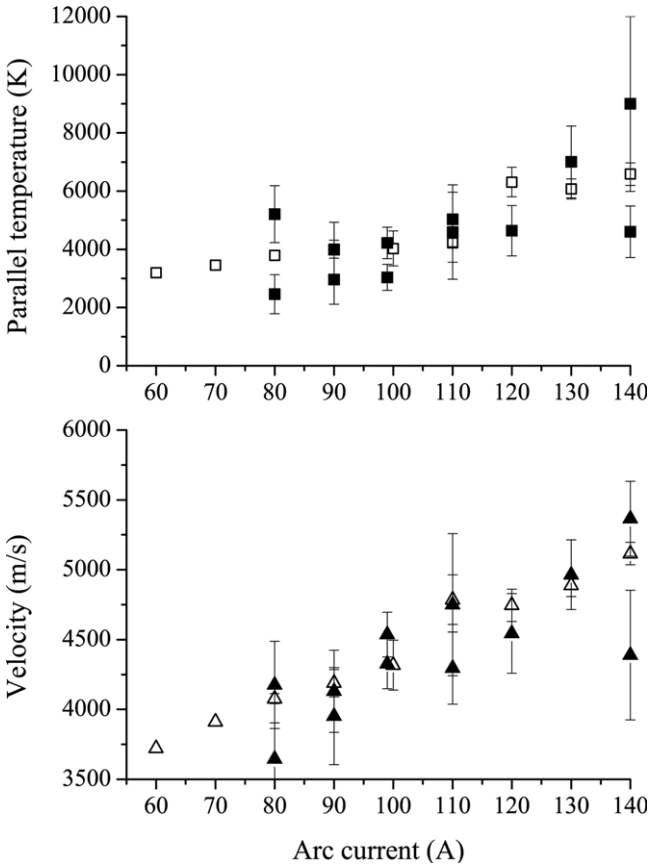

Figure 10. Evolution of the oxygen atom parallel temperature and axial velocity with the arc current at the nozzle exit for a CO_2 (full symbols) and a CO_2–N_2 (open symbols) plasma expansion.

5000 m s^{-1} is found in experiments for a power of 9 kW, as shown in figure 10. Typically, a space probe enters the upper layers of the Martian atmosphere at a speed of 8 km s^{-1} before aerobreaking or aerocapture maneuvre [1, 2]. Assuming that the torch behaviour is not affected by a very high current, one finds that 310 A is necessary to obtain $v_x = 8000$ m s^{-1} by extrapolating data presented in figure 10. Meanwhile, the temperature at the nozzle outlet reaches 13 000 K. Therefore, the study indicates that a power of about 20 kW is necessary to properly reproduce a Mars entry in terms of spacecraft speed when an arcjet is employed. Such a number is reasonable; however, the torch as well as the vacuum chamber must be designed to withstand very high powers for long durations.

6. Conclusion

The LIF technique is perfectly suited for the examination of the properties of the VDFs of $^5S_2^o$ metastable oxygen atoms in rarefied CO_2 supersonic plasma expansions. The measured atomic lineshapes allow one to compute the mean velocity and the temperature in the perpendicular and parallel directions with respect to the jet axis. The distribution of flow parameters reveals the existence of a barrel shock wave and a stationary shock front, which originate in shock wave regular reflection under current experimental conditions. Investigation of the effect of the applied power upon the plasma flow properties

shows that one way to achieve a high velocity is to pass a large current though the gas. That, however, necessitates the design of an appropriate torch.

This work indicates that CO_2 supersonic plasma flows can be used to experimentally simulate entry conditions in the upper layers of the Martian atmosphere in terms of pressure and flow velocity; however, a large power is required. On the contrary, the chemical composition of the plasma flow does not correspond to the one encountered ahead of the shock wave that surrounds a spacecraft. Validation of the Martian chemistry therefore demands dedicated experiments.

The continuation of this study can be divided into two parts. The measurement of the velocity and temperature of molecular fragments like CO, NO and N_2 first comes to mind. The determination of the molecule vibrational and rotational temperature is of specific interest in order to better quantify the energy content of the plasma expansion. Besides, a comparison between experimental data and computer simulations outcomes based on existing two-temperature plasma models appears necessary in order to validate the set of chemical reactions introduced into modelling of probe entry into the Martian atmosphere.

References

[1] Landau D F and Longuski J M 2007 *J. Spacecr. Rockets* **44** 203
[2] Landau D F and Longuski J M 2006 *J. Spacecr. Rockets* **43** 1035
[3] Gallis M A and Harvey J K 1995 Analysis of non-equilibrium in Mars atmosphere entry flows *30th Thermophysics Conf.* (*San Diego, CA*) AIAA paper 95-2095
[4] Mazouffre S, Lago V, Lino da Silva M, Dudeck M and Pawelec E 2002 Plasma formation during high speed flights in upper layers of the Earth's atmosphere *11th Int. Conf. on Space Plane and Hypersonic Systems and Technologies* (*Orléans, France*) AIAA paper 02-5272
[5] Park C, Howe J T and Jaffe L 1994 *J. Thermophys. Heat Transfer* **8** 9
[6] Magin T, Degrez G and Sokolova I 2002 Thermodynamic and transport properties of Martian atmosphere for space entry applications *33rd Plasmadynamics and Lasers Conf.* (*Maui, Hawai*) AIAA paper 02-2226
[7] Gindrat M, Dorier J-L, Hollenstein Ch, Refke A and Barbezat G 2004 *Plasma Sources Sci. Technol.* **13** 484 and references therein
[8] Baer D S, Crasg H A and Hanson R K 1993 *J. Quant. Spectrosc. Radiat. Transfer* **50** 621
[9] Matsui M, Takayanagi H, Oda Y, Komurasaki K and Arakawa Y 2004 *Vacuum* **73** 341
[10] Miller D R 1988 *Atomic and Molecular Beam Methods* ed G Scoles (Oxford: Oxford University)
[11] Schram D C, Mazouffre S, Engeln R and van de Sanden M C M 2001 *Atomic and Molecular Beams* ed R Campargue (Berlin: Springer) p 209
[12] Graur I A, Lengrand J C and Elizarova T G 2000, *Proc. 22nd Int. Symp. on Shock Waves* (*London*) vol 2 ed G J Ball *et al* (London: Imperial College) p 1267
[13] Ivanov M S, Markelov G N, Kudryavtsev A N and Gimelshein S F 1998 *AIAA J.* **36** 2079
[14] Ivanov M S, Vandromme D, Fomin V M, Kudryavtsev A N, Hadjadj A and Khotyanovsky D V 2001 *Shock Waves* **11** 199
[15] Mazouffre S, Caubet-Hilloutou V and Lengrand J C 2005 *Plasma Sources Sci. Technol.* **12** 012323
[16] Lago V 2008 private communication
[17] Lino da Silva M, Passarinho F an Dudeck M 2006 *J. Thermophys. Heat Tranfer* **20** 680
[18] Mazouffre S and Pawelec E 2007 Metastable oxygen atom velocity and temperature in expanding CO_2 plasma jets *28th Int. Conf. on Phenomena in Ionized Gases* (*Prague, Czech Republic*) paper 4P06-08
[19] Engeln R, S Mazouffre, Vankan P, Schram D C and Sadeghi N 2001 *Plasma Sources Sci. Technol.* **10** 595
[20] Vankan P, Mazouffre S, Schram D C and Engeln R 2005 *Phys. Plasmas* **12** 102303
[21] Demtröder W 1998 *Laser Spectroscopy* (New York: Springer)
[22] Pak I and Sadeghi N 1995 Radiative lifetime of the $O(^5S_2)$ metastable state and collisional coupling between the $O(^5P_{1,2,3})$ fine structure sub-levels *Proc. 48th Gaseous Electronic Conf. (Berkeley, CA), Am. Phys. Soc. Bull.* **40**
[23] Mori T, Kanou K, Mizuta K, Kuramasu T, Ishikawa Y and Arai S 1992 *J. Chem. Phys.* **97** 9094
[24] Lee J S and Bobbitt P J 1969 Transport properties at high temperatures of CO_2–N_2–O_2–Ar gas mixtures for planetary entry applications *NASA Technical Note* TN D-5476
[25] Barbosa E, Lopez B, Dudeck M, Kaminska A and Izrar B 2007 Numerical simulation of non-equilibrium hypersonic flow in a convergent–divergent nozzle: application to Mars atmospheric entry simulation *Proc. 8th Int. Symp. on Experimental and Computational Aerothermodynamics of Internal Flows* (*Lyon, France*) paper 0041